Planetary and Space Science 135 (2017) 27–36

Contents lists available at ScienceDirect

Planetary and Space Science

journal homepage: www.elsevier.com/locate/pss

Oblique impact cratering experiments in brittle targets: Implications for elliptical craters on the Moon

Tatsuhiro Michikami[a,*], Axel Hagermann[b], Tomokatsu Morota[c], Junichi Haruyama[d], Sunao Hasegawa[d]

[a] Faculty of Engineering, Kindai University, Hiroshima Campus, 1 Takaya Umenobe, Higashi-Hiroshima, Hiroshima 739-2116, Japan
[b] Department of Physical Sciences, The Open University, Walton Hall, Milton Keynes MK7 6AA, United Kingdom
[c] Graduate School of Environmental Sciences, Nagoya University, Furo, Chikusa, Nagoya, Aichi 464-8602, Japan
[d] Institute of Space and Astronautical Science, Japan Aerospace Exploration Agency, Sagamihara, Kanagawa 252-8510, Japan

ARTICLE INFO

Keywords:
Oblique impact cratering process
Pit crater
Moon
Elliptical crater
Laboratory experiments

ABSTRACT

Most impact craters observed on planetary bodies are the results of oblique impacts of meteoroids. To date, however, there have only been very few laboratory oblique impact experiments for analogue targets relevant to the surfaces of extraterrestrial bodies. In particular, there is a lack of laboratory oblique impact experiments into brittle targets with a material strength on the order of 1 MPa, with the exception of ice. A strength on the order of 1 MPa is considered to be the corresponding material strength for the formation of craters in the 100 m size range on the Moon. Impact craters are elliptical if the meteoroid's trajectory is below a certain threshold angle of incidence, and it is known that the threshold angle depends largely on the material strength. Therefore, we examined the threshold angle required to produce elliptical craters in laboratory impact experiments into brittle targets. This work aims to constrain current interpretations of lunar elliptical craters and pit craters with sizes below a hundred meters. We produced mortar targets with compressive strength of 3.2 MPa. A spherical nylon projectile (diameter 7.14 mm) was shot into the target surface at a nominal velocity of 2.3 km/s, with an impact angle of 5°-90° from horizontal. The threshold angle of this experiment ranges from 15° to 20°. We confirmed that our experimental data agree with previous empirical equations in terms of the cratering efficiency and the threshold impact angle. In addition, in order to simulate the relatively large lunar pit craters related to underground cavities, we conducted a second series of experiments under similar impact conditions using targets with an underground rectangular cavity. Size and outline of craters that created a hole are similar to those of craters without a hole. Moreover, when observed from an oblique angle, a crater with a hole has a topography that resembles the lunar pit craters. The relation between the impact velocity of meteoroids on the Moon and the probability of elliptical crater formation was investigated based on our experimental results and an existing empirical equation. The results suggest a distinct possibility that most craters in the 100 m size range on the Moon, given their elliptical shape, originated as secondary craters.

1. Introduction

Impact craters are the dominant features on solid-surface planetary bodies in the solar system. Most impacts on solid-surface planetary bodies occur at an oblique angle of incidence, and it has long been known that the most likely angle of incidence is 45° (e.g., Shoemaker, 1962). Impacts at a very shallow angle to the surfaces produce elliptical craters: if an impactor strikes the planetary surface at an angle less than a certain threshold angle, the resulting crater shape is not a circular and becomes elongated in the direction of impact. Only roughly 5% of all craters (greater than 1 km in diameter) observed on Mars, Venus, and the Moon have elliptical shapes with an ellipticity of 1.1 or greater, where the crater's ellipticity is defined as the ratio of its maximum and minimum rim-to-rim diameters (Bottke et al., 2000). Although elliptical impact craters may be rare on solid-surface planetary bodies, a better understanding of the formation of elliptical craters would contribute to our overall understanding of impact cratering. For instance, it is well-known that crater size depends on impact angle (e.g., Elbeshausen et al., 2009).

Recently, more and more craters in the 100 m size range have been observed on Mars and the Moon by the telescopic camera on board Mars Reconnaissance Orbiter and the Lunar Reconnaissance Orbiter

* Corresponding author.
E-mail address: michikami@hiro.kindai.ac.jp (T. Michikami).

http://dx.doi.org/10.1016/j.pss.2016.11.004
Received 2 July 2016; Accepted 20 November 2016
Available online 24 November 2016
0032-0633/ © 2016 The Authors. Published by Elsevier Ltd.
This is an open access article under the CC BY license (http://creativecommons.org/licenses/BY/4.0/).

Camera (LROC), respectively. These data reveal the variety of crater shapes on Mars and the Moon. Among some smaller craters observed on Mars and the Moon, deep pit craters are occasionally seen (e.g., Cushing, 2012; Robinson et al., 2012). These craters, characterized by their steep walls, are generally considered to be the results of roof collapses into subsurface cavities. On the Moon, deep pit craters with a diameter of more than 50 m were discovered in SELenological and Engineering Explorer (SELENE) Terrain Camera (TC) images (Haruyama et al., 2009, 2012) and were investigated in detail by LROC (Robinson et al., 2012). These deep pit craters are generally called Marius Hill Pit, Mare Tranquillitatis Pit and Mare Ingenii Pit. There are often called 'deep pit craters, 'deep pits', or 'holes'. In this study, we will simply refer to them as 'pit craters'. One possibility for their formation was the collapse of the roof of an underground cavity such as a lava tube, brought about by a random meteoroid impact (Haruyama et al., 2009, 2012: Martellato et al., 2013: Michikami et al., 2014). These maximum and minimum pit diameters are 57 and 48 m for Marius Hill Pit, 99 and 84 m for Mare Tranquillitatis Pit, and 103 and 66 m for Mare Ingenii Pit; the shapes of these pit craters are elliptical. In order to investigate the formation of Martian pit craters, Michikami et al. (2014) carried out impact experiments into brittle targets with a cavity at an impact angle of 90° from the horizontal, resulting in circular craters. However, the elliptical shapes of lunar pit craters cannot be explained by the data of Michikami et al. (2014). Therefore, it is necessary to carry out oblique impact experiments into brittle targets with a cavity.

Laboratory oblique impact cratering experiments into targets with a strength relevant to the surface of extraterrestrial bodies are still sparse, although there have been a number of studies of oblique cratering, both in experiments and modelling. Among the oblique impact experiments conducted, those of Gault (1973) and Gault and Wedekind (1978) are most widely known. They reported on impacts into granite and sand. Crater formation is generally divided into two regimes, the strength and the gravity regime, depending on which of the two effects dominates during cratering. The impacts into granite simulated impacts in the strength regime; those into sand were done to investigate impacts in the gravity regime. They found that the ellipticity of the crater increases with decreasing impact angle from the horizontal of the target surface. For instance, projectiles fired at an angle of 4.75° from the horizontal or less into sand targets produce an elliptical crater with an ellipticity greater than 1.1. Unfortunately, on rock targets, no data were given for impacts at angles less than 15° from the horizontal. In order to investigate the effect of impact angle on crater ellipticity in rock, Burchell and Whitehorn (2003) (From now on, we will abbreviate this to "BW03") carried out the oblique impact experiments in granite targets. They found that crater depth and excavated mass start to decrease immediately when non-normal incidence occurs. Their results suggest that projectiles shot at angle 10° from the horizontal or less into granite targets produce elliptical craters with ellipticities greater than 1.1.

As mentioned above, although several laboratory experiments have been conducted to simulate oblique impacts under conditions relevant to planetary surfaces, experimental data are insufficient as analogues for craters in the 100 m size range. Impact craters larger than a kilometer on the Moon would occur in the gravity regime (e.g., Holsapple and Schmidt, 1979; Collins et al., 2011). On the other hand, impact craters smaller than a hundred meters on the Moon would occur in the strength regime (e.g., Stöffler et al., 2006; Daubar et al., 2014). In the past experiments, for an example, the strength (a general compressive strength ~ a few hundred MPa) of granite targets adopted by BW03 would be larger than that of a planetary surface, which is admittedly not very well characterized, but is thought to be on the order of 1 MPa (e.g., Melosh, 1989; Collins et al., 2011; Daubar et al., 2014). Besides, both laboratory experiments (Gault and Wedekind, 1978; Christiansen et al., 1993; Burchell and Mackay, 1998; Burchell and Whitehorn, 2003) and numerical simulations (Collins et al., 2011) revealed that the angle below which elliptical craters form, the so-called threshold angle, depends on the properties of the target material. Therefore, it is important to simulate oblique impacts under conditions relevant craters in the 100 m size range by using brittle target with a strength on the order of 1 MPa.

The purpose of this study is twofold: our first aim is to examine the threshold impact angle for producing elliptical craters in the 100 m size range on the Moon. For this purpose, we carried out oblique impact experiments into mortar targets with a strength on the order of 1 MPa (Section 3.1). In Section 4.1, we compare our experimental results with previous studies for various target materials, e.g. the data of Grey et al. (2002), who report on laboratory oblique impact experiments into ice targets with a similar strength. We consider the influence of both target material and impact velocity because, according to previous studies (e.g., Collins et al., 2011; Elbeshausen et al., 2013), the threshold impact angles are strongly affected by not only the target material but also by the impact velocity. In Section 4.2, we then apply our experimental results to elliptical craters on the Moon, by investigating the effect of impact angle on elliptical crater formation at various impact velocities.

Our second aim is to explore the formation of lunar pit craters with elliptical shapes. For this purpose, we carried out oblique impact experiments for mortar targets with a cavity (Section 3.2). The craters in targets with and without cavity are compared in Section 3.3. We take a look at the relation between the craters in targets with a cavity and three pit craters on the Moon in Section 4.3. Finally, we present conclusions in Section 5.

2. Experimental procedures

2.1. Target production method and target properties

The targets were produced using same methods as described by Michikami et al. (2014). They were fabricated using a mixture of cement, water and Toyoura sand (an engineering standard-sand in Japan) in the ratio of 1:1:10, by weight. The particle size of the sand is about 0.2 mm. The mixture was then put in a mold and was compacted. In order to simulate the formation of elliptical craters and elliptical pit craters on the Moon, we produced targets without and with a rectangular cavity using two molds. Rectangular parallelepiped target with a length 20 cm, width 20 cm and height 6 cm, without a cavity, were produced to simulate elliptical craters. In order to simulate elliptical pit craters, rectangular parallelepiped target with a length 35 cm, width 25 cm and height 4 cm were produced, and a rectangular cavity was set into the target underground to yield a cuboid as shown in Fig. 1 (the roof thickness is 1 cm). After a few days, the mold was taken off and the targets were left to air-dry for about one week. In the end, both types of target had a bulk density of 1550 kg/m^3, a porosity of ~40%, a compressive strength of 3.2 MPa, and a tensile strength of 0.83 MPa (for more detail, refer to Michikami et al., 2014).

2.2. Impact experiments

The impacts were carried out using a two-stage light-gas gun at the Institute of Space and Astronautical Science, Japan Aerospace Exploration Agency (ISAS, JAXA). Seven oblique impact experiments for the targets without a cavity were performed at impact angles from 5° (glancing shot) to 90° (vertical shot) from the horizontal were performed and seven oblique impact experiments for the targets with a cavity were carried out at impact angles from 2° to 90° from the horizontal (Tables 1, 2). Spherical nylon projectiles 7.14 mm in diameter (mass 0.217 g and density 1140 kg/m^3) were fired into the target surface at a nominal impact velocity of 2.3 km/s. The impact velocities in the experiments with impact angle of 90° from the horizontal were exceptional in that they were slightly faster (2.44 km/s for s1941 and 2.62 km/s for s806) than those in the other

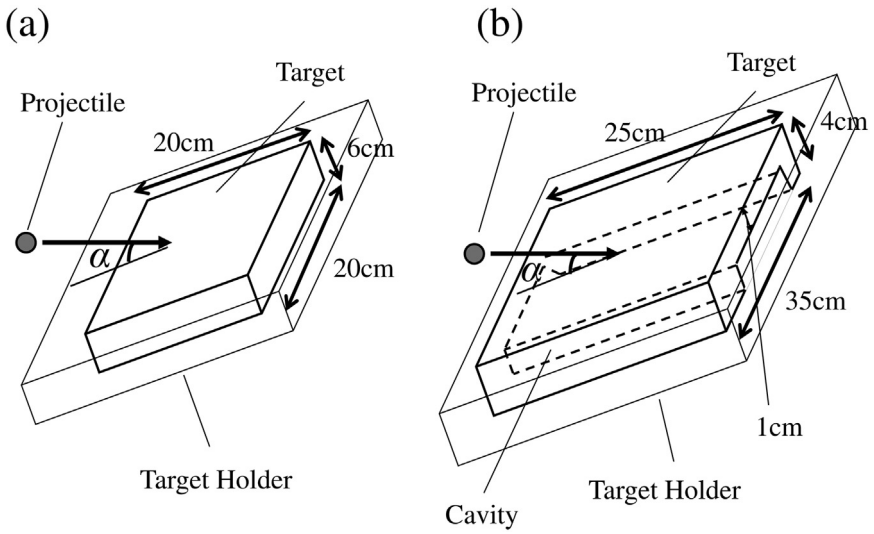

Fig. 1. Configuration of experimental setup. (a) Target without cavity; (b) Target with cavity. The impact angle α is defined as the angle between projectile trajectory and target surface.

Table 1
Elliptical craters observed in mortar targets without a cavity. Length is the maximum dimension of the crater in line with the projectile trajectory, and width is the maximum one orthogonal to the projectile trajectory.

Shot number	Impact angle	Length [cm]	Width [cm]	Depth [cm]	Crater volume [cm^3]	Ellipticity [Length/Width]	Impact velocity [km/s]
s1933	5°	4.5 ± 0.1	1.8 ± 0.1	0.50 ± 0.02	1.01 ± 0.05	2.5	2.29
s1308	10°	3.9 ± 0.1	2.0 ± 0.1	0.51 ± 0.02	1.03 ± 0.05	2.0	2.26
s1936	15°	3.5 ± 0.1	2.8 ± 0.1	0.60 ± 0.02	1.67 ± 0.05	1.3	2.35
s1942	20°	3.5 ± 0.1	3.4 ± 0.1	0.95 ± 0.02	3.20 ± 0.05	1.0	2.35
s1935	30°	3.8 ± 0.1	4.0 ± 0.1	1.00 ± 0.02	4.70 ± 0.05	1.0	2.23
s1939	45°	4.8 ± 0.1	4.6 ± 0.1	0.94 ± 0.02	8.09 ± 0.05	1.0	2.29
s1941	90°	6.3 ± 0.1	5.4 ± 0.1	1.15 ± 0.02	11.10 ± 0.05	1.2	2.44

oblique impact experiments. Impact velocities were obtained from the passage time of the projectile between two laser beams. The targets were enclosed in a target holder with the front surface fully exposed on the impact side. The ambient pressure in the chamber was less than 100 Pa. The reproducibility of the resulting crater (or pit crater) in the type of mortar targets used in these experiments has been confirmed by the experiments of Michikami et al. (2014) which were carried out using identical mortar targets.

The resulting crater and pit crater, after each shot, were measured to yield its maximum depth, length (maximum dimension of the crater in line with the projectile trajectory), width (maximum dimension of the crater orthogonal to the projectile trajectory) with digital calipers. The volume of the crater without a hole was measured using 3D laser scanner "E-Measure3D" (COMS. Co, Ltd). We also measured depth, length, and width of the crater without a hole using "E-Measure3D", but the results only confirmed the digital caliper measurements. We did not measure the crater with a hole using "E-Measure3D" because some targets broke in transit (caliper measurements of the craters were finished before transport). Thus, with the exception of crater volume, we adopted the value obtained with digital calipers.

3. Results

3.1. Oblique impacts into targets without a cavity

We observed a large range of crater shapes in targets without a cavity for various impact angles 5°-90° from the horizontal). Fig. 2 shows photographs of the elliptical craters obtained in the experiments. The data for these impacts are given in Table 1. In Fig. 2, the ellipticity of the crater increases with decreasing impact angle. The same

Table 2
Elliptical craters observed in mortar targets with a cavity.

Front crater					Rear crater			Hole		
Shot number	Impact angle	Length [cm]	Width [cm]	Ellipticity [Length/Width]	Length [cm]	Width [cm]	Ellipticity [Length/Width]	Length [cm]	Width [cm]	Ellipticity [Length/Width]	Impact velocity [km/s]
s1711	2°	4.7 ± 0.1	1.0 ± 0.1	4.7	4.0 ± 0.1	3.3 ± 0.1	1.2				2.33
s1713	5°	4.5 ± 0.1	2.2 ± 0.1	2.0	4.3 ± 0.1	4.0 ± 0.1	1.1	2.8 ± 0.1	1.4 ± 0.1	2.0	2.39
s1306	10°	4.0 ± 0.1	2.4 ± 0.1	1.7	4.8 ± 0.1	3.3 ± 0.1	1.5	2.5 ± 0.1	1.3 ± 0.1	1.9	2.35
s1712	15°	3.8 ± 0.1	3.0 ± 0.1	1.3	4.5 ± 0.1	4.1 ± 0.1	1.1	2.6 ± 0.1	1.8 ± 0.1	1.4	2.39
s1305	20°	3.7 ± 0.1	3.5 ± 0.1	1.1	5.3 ± 0.1	5.2 ± 0.1	1.0	2.6 ± 0.1	2.2 ± 0.1	1.2	2.38
s1309	30°	4.3 ± 0.1	4.0 ± 0.1	1.1	5.3 ± 0.1	5.0 ± 0.1	1.1	2.8 ± 0.1	2.7 ± 0.1	1.0	2.38
s806	90°	5.2 ± 0.1	4.9 ± 0.1	1.1	5.5 ± 0.1	5.4 ± 0.1	1.0	3.4 ± 0.1	3.3 ± 0.1	1.0	2.62

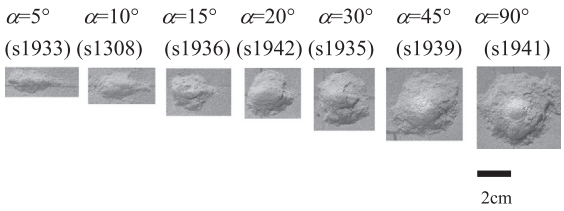

Fig. 2. Photographs of elliptical craters created by impacts into targets without a cavity at various impact angles. Projectiles came from the left of the photograph.

tendency was shown in the oblique impact experiments into granite (Burchell and Whitehorn, 2003). In our experiments, although the impact conditions (impact velocity, projectile and target material) are different, crater sizes are similar to those in BW03. Thus, it is easier to compare our data to theirs. Fig. 3 shows our and BW03's data of crater measurements graphically (crater depth, length, width and crater volume).

In Fig. 3, crater depth appears to increase with increasing impact angle. The data of BW03 shows that crater depth increases with the sine of impact angle to the power 0.5. Our data are somewhat scattered in the impact angle (The cause may be the roughness seen around the bottom of each crater). Crater lengths in our and BW03's data appear to decrease with decreasing impact angle down to 20° and 10°, respectively, and then increase again for even shallower impacts, i.e. the crater lengths show a V-shaped trend. As pointed out by Elbeshausen et al. (2013), an oblique impact deposits its energy less deep into the target and as a result the crater length decreases with decreasing impact angle at higher impact angles. On the other hand, the length increase at lower impact angles can be attributed to the secondary structure generated by projectile sliding along the target surface downrange. Crater width increases with increasing impact angle, and our data agree well with BW03's data. Crater volume scales linearly with sinα in the data of BW03. In our data, the slope of crater volume vs impact angle is steeper than that of BW03.

Fig. 4 shows the ellipticity of the craters vs impact angle. The ellipticity of the crater is almost constant and near 1 (the craters are circular) in the range of more than 10°-20°. The ellipticities of the craters increase dramatically with decreasing impact angle once the threshold angle falls below approx. 15°-20°. In experiments of BW03, an elliptical crater with an ellipticity of 1.1 is formed at an impact angle of 10° (the threshold angle). In our experiments, the craters formed at impact angles of 15° and 20° have ellipticities of 1.3 and 1.0, respectively. Hence, the threshold angle for the formation of elliptical

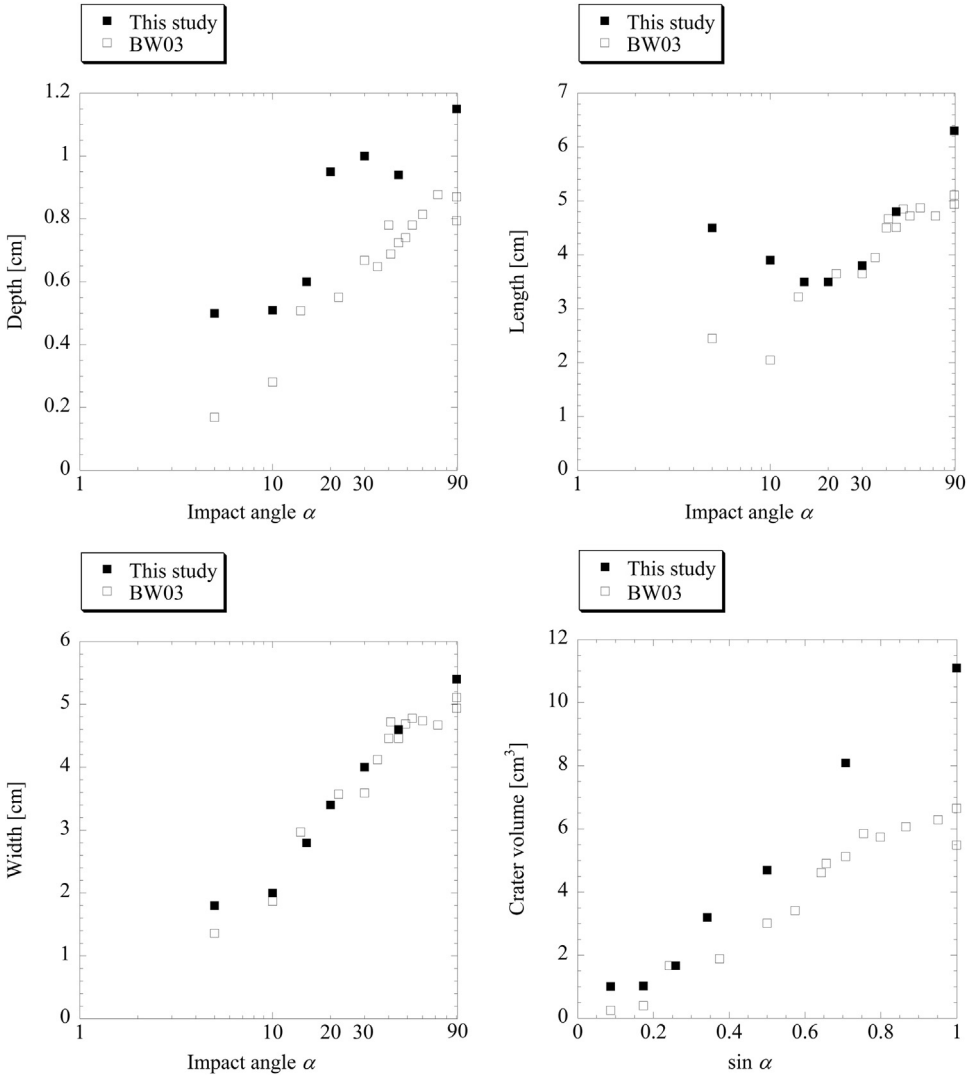

Fig. 3. Crater depth, length, width and crater volume vs impact angle, plotted for the laboratory impact experiments of this study and BW03 (Burchell and Whitehorn, 2003). We fired nylon projectile spheres into mortar targets at a nominal velocity of 2.3 km/s. BW03 fired stainless-steel spheres into granite targets at a nominal velocity of 5.4 km/s. The error bars are not shown in the figure because almost all error bars are smaller than the symbol size. The crater volumes of BW03 were calculated by weighing the excavated mass (from the crater) and dividing it by the granite's density of 2.75 g/cm^3.

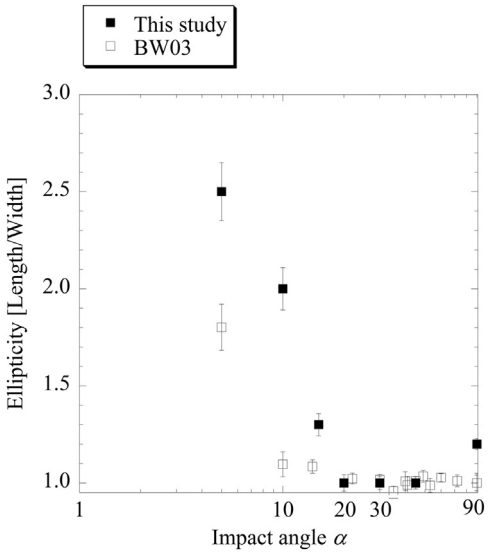

Fig. 4. Ellipticity of craters vs impact angle, plotted for the laboratory impact experiments of this study and BW03 (Burchell and Whitehorn, 2003).

crater in our experiments can be assumed to lie between 15° and 20°, which is slightly greater than that of 10° in BW03. We discuss the reason for this in Section 4.1.

3.2. Oblique impacts into targets with a cavity

In addition to the craters in targets without a cavity, a large range of pit craters in targets with a cavity (roof thickness is 1 cm) was observed for various impact angles (2°-90° from the horizontal). Fig. 5 shows photographs of the elliptical craters in targets with a cavity. The pit craters were observed at the impact angle of 5°-90° from the horizontal. In these experiments, we observed that a crater was produced on the opposite side of the target with respect to the impact. In the following, we refer to the crater formed on the impact surface as 'front crater' and to the crater formed on the opposite surface as 'rear crater'. Penetration of the target was achieved when both of these craters were connected to form a continuous hole (cf. Michikami et al., 2014). In the experiments with an impact angle of 2° (s1711), the front and rear craters were not connected and as a result the pit crater was not seen, which was exceptional. For impact angles of 30° and 90°, the shapes of the front craters and the holes are close to circular, i.e. their ellipticities are similar. For the impact angles less than 20°, on the other hand, these shapes gradually become elongated as the impact angles decrease. Most rear craters appear to be slightly bigger in size than the front craters.

In order to understand these craters shapes quantitatively, lengths and widths of front craters, rear craters and holes are shown in Fig. 6. In each case, the width decreases with decreasing impact angle. On the other hand, the lengths of the front crater and the hole remain roughly constant regardless of impact angle, although these data show a slight V-shaped trend as well as the craters without a hole. Consequently, the shapes of the front crater and the hole gradually become elongated as the impact angle decreases. The rear crater's length and width both only decrease slightly with decreasing impact angle. Therefore, it is fair to say that the shape of the rear crater does not change significantly in terms of the impact angle.

The above can be confirmed by comparing ellipticities. Fig. 7 shows the ellipticities of front crater, rear crater, and hole vs the impact angle. Overall, the ellipticities of front crater and hole are similar, and increase with decreasing impact angle, whereas that of the rear crater is almost constant regardless of impact angle. Above 20°, the ellipticities of front and rear craters are almost constant and near unity (the craters are almost circular). The tendency is similar to that observed for craters without a hole shown in Fig. 4. The front crater formed at the impact angle of 15° has an ellipticity of 1.3 whilst the elipticity of the hole formed at the impact angle of 20° is 1.2. The threshold angle of elliptical shape in the front crater and the hole would be around 20°, the same value we found for craters without a hole.

3.3. Comparison of craters in targets with and without cavity

Lengths, widths and ellipticities of the craters (or front craters) in both types of targets are shown in Fig. 8. Comparing these values we find they are very similar, i.e. size and shape of craters created at the same impact angle are similar, regardless of the existence of a hole. Note that this result has not been found in previous experiments, because no laboratory oblique impact experiments into brittle targets with a cavity have been reported in the literature. Of course, in the target with a cavity, the target roof thickness affects the crater formation. The effect of target roof thickness on crater formation has already been investigated by Michikami et al. (2014). Their study showed that the diameter of front craters remains almost constant regardless of target roof thickness, and the diameter of the holes created decreases with increasing target roof thickness. However, the shapes of front crater and hole do not change in terms of target roof thickness.

4. Discussion

4.1. Comparison with targets made of other materials

In order to put our results into context, we compare our experiments with previous oblique impact experiments for various target materials. Gault and Wedekind (1978), Grey et al. (2002), and Christiansen et al. (1993) (hereafter abbreviated to "GW78", "G02" and "C93", respectively) fired projectiles into sand, ice and aluminum targets at various

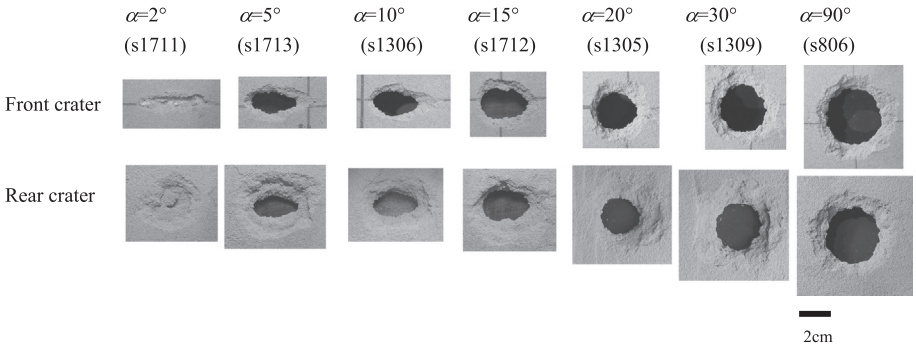

Fig. 5. Photographs of elliptical craters for impacts into targets with a cavity at various impact angles. Projectiles came from the left of the photograph. Craters were produced on the opposite side of the target with respect to the impact. In this paper, we refer to the crater formed on the impact surface as 'front crater' and to the crater formed on the opposite surface as 'rear crater'. Exceptionally, the roof overlaying the cavity was not penetrated in shot s1711 ($\alpha = 2^{\circ}$).

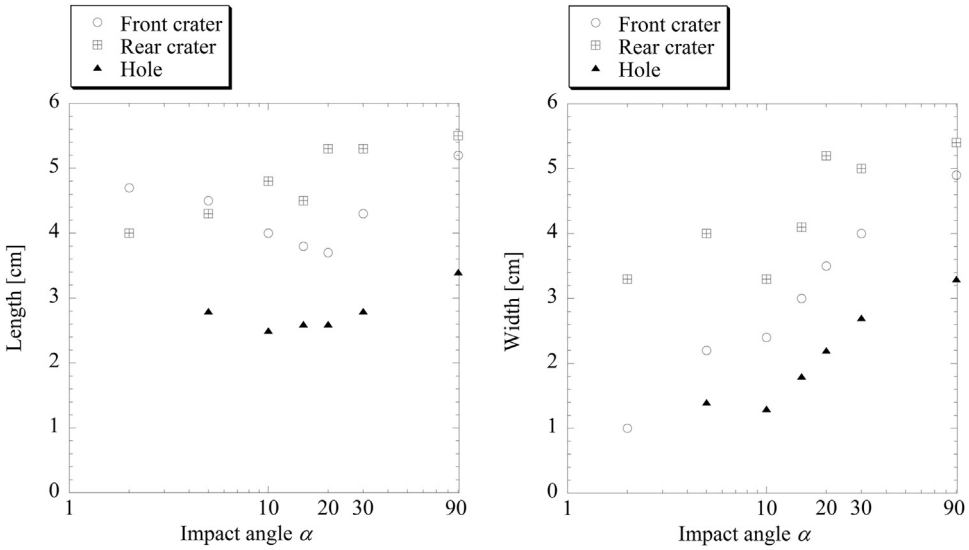

Fig. 6. Length and width of front crater, rear crater and hole vs impact angle. The error bars are omitted as they are smaller than the symbol sizes.

impact angles. Fig. 9 shows crater ellipticity vs impact angle for various target materials. The ellipticity of the crater remains almost constant above a threshold impact angle that is dependent on the target material. The threshold impact angles of the sand, mortar, granite and aluminum targets are 5°, 15–20°, 10° and 25°, respectively.

In the case of ice targets, it may be difficult to determine the threshold impact angle because the outlines of craters have irregularities due to large spall fragments. For instance, a crater produced at an impact angle of 15° has a greater ellipticity (1.4) than a crater produced at an impact angle of 10° (1.1). In addition, there is no data for impact angles below 10°. Therefore, the threshold angle of ice targets would be 15° or 10° or less. For the sake of simplicity, the threshold angle of the ice target is assumed to lie between 5° and 15° in this study.

Listing the targets in order of increasing structural strength, we can compare sand, mortar (ice), granite and aluminum. Here, the compressive strength of ice targets is generally several MPa (cf. Fig. 4 in Schulson, 1999), which is similar to that of our mortar targets. The threshold impact angle tends to increase with increasing target strength, with the exception of our data: at 15°-20°, the threshold impact angle of our mortar targets is greater than that of granite 10°, although our targets are weaker. Our threshold impact angle appears to be slightly greater than that of ice (5°-15°), although our targets have a similar strength. A possible explanation is that the threshold impact angle is strongly affected by impact velocity (e.g., Collins et al., 2011; Elbeshausen et al., 2013). GW78, G02, BW03, and C93 conducted impact experiments at 6.4 km/s, 5.2 km/s, 5.4 km/s and 6.5–7.0 km/s, respectively, so their impact velocities do not differ largely. On the other hand, our experiments were carried out at 2.3 km/s, less than half of BW03's. Impacts at a lower velocity result in lower cratering efficiency, i.e. the ratio of crater to projectile diameter. Therefore, the threshold impact angle of our experiments cannot be simply compared with previous data.

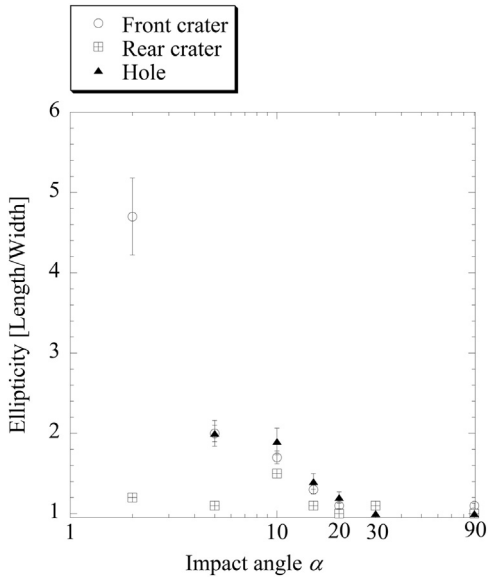

Fig. 7. Ellipticities of front crater, rear crater and hole vs impact angle. As before, error bars smaller than the symbol size are omitted.

Based on the results of numerical simulations and laboratory experiments of oblique crater formation, Collins et al. (2011) indicated that the threshold angle for the formation of elliptical craters is a function of cratering efficiency. Fig. 10 shows the threshold impact angle as a function of cratering efficiency. In addition to our experimental results, the results of previous laboratory experiments are plotted. The threshold angle as a function of cratering efficiency follows a single trend. Three different empirical equations have been proposed for this single trend by Bottke et al. (2000), Collins et al. (2011) and Elbeshausen et al. (2013), respectively. All three empirical equations agree with the experimental data, as shown in Fig. 10. The experimental results shown comprise laboratory impact experiments into sand, mortar, ice, granite, lead and aluminum, a data range covering orders of magnitude in terms of crater scales, all the way from the gravity regime to the strength regime. The empirical equations are independent of the cratering regime (strength and gravity regimes).

4.2. Implications for elliptical craters on the Moon

The data presented here can help understand the origin of elliptical craters on the Moon, as long as the evidence is interpreted carefully. As mentioned before, crater in the 100 m size range on the Moon are produced in the strength regime. More specifically, the relative influence of gravity and strength can be measured by the ratio $S = Y/\rho gL$ (Y is cohesive strength, ρ is the density, g is gravity and L is impactor diameter). A large S value means that the crater is produced in the strength regime; a small S indicates that the crater is produced in the gravity regime. According to Collins et al. (2011), cratering would occur in the strength regime for S greater than 10; when S is less than 0.1, cratering would occur in the gravity regime. In the case of 100 m sized lunar craters, the most appropriate parameters are: $Y = 1$ MPa, $\rho = 2500$ kg/m^3, $g = 1.62$ m/s^2, and $L = 10$ m (Holsapple, 1993; Melosh,

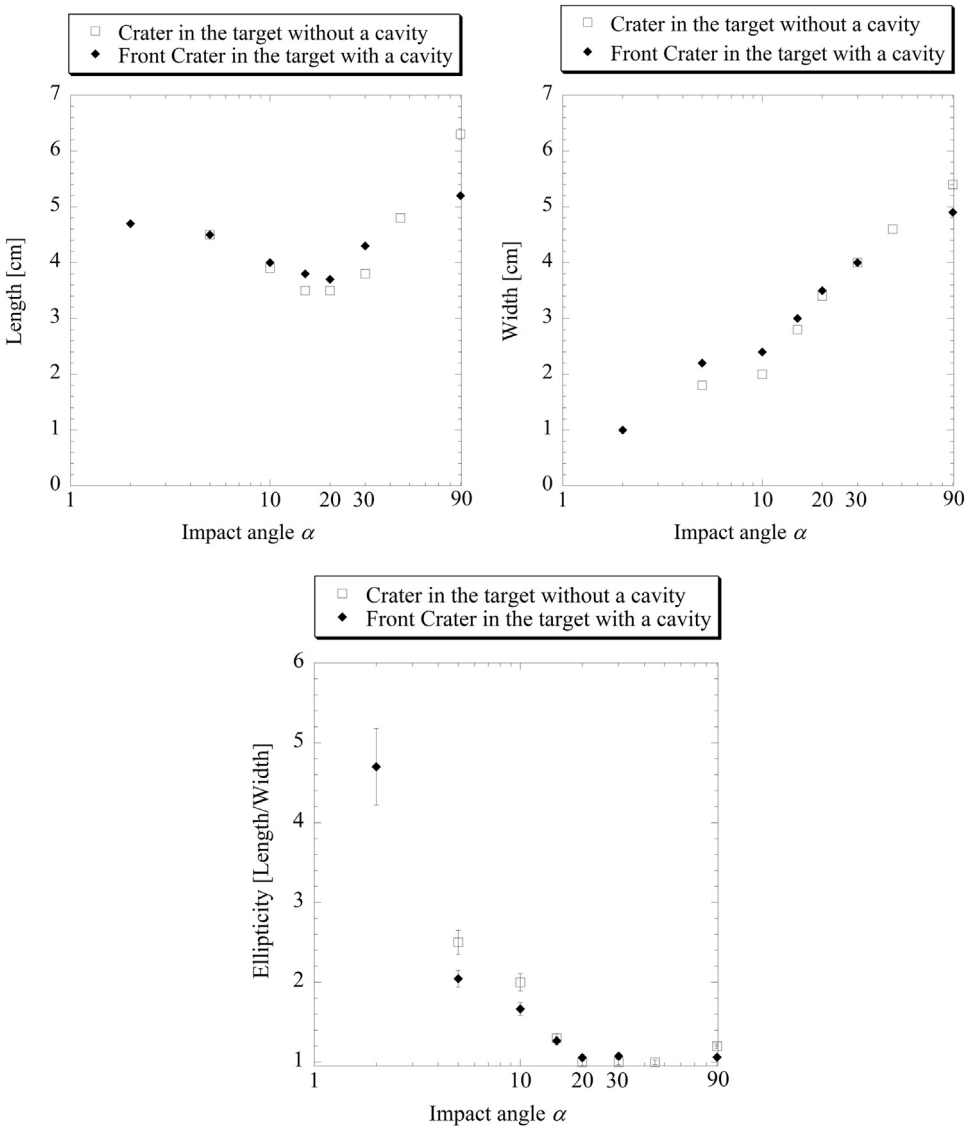

Fig. 8. Crater length, width and ellipticity vs impact angle. For targets with a cavity, the measurements refer to the front. Error bars smaller than the symbol size are omitted.

1989). The resulting estimate for S is 25 (> 10), so the formation of the lunar craters in question would have been strength-dominated. Other studies (e.g., Stöffler et al., 2006; Daubar et al., 2014) indicated a similar estimate.

As mentioned before, for the same material, impact velocity affects cratering efficiency, and consequently, influences the threshold angle of elliptical crater formation. Besides, as the secondary craters observed on the Moon have been produced by low velocity impacts, the corresponding cratering efficiency must have been relatively low compared with that of primary craters. Hence, secondary craters are more likely to be elliptical. Based on the empirical equations above and our experimental results, we now take a look at the relation between the impact velocity of meteoroids on the Moon and the probability of elliptical crater formation,.

Holsapple's (1993) scaling law is used because it applies to impact cratering in a wide scale range and is most widely adopted. In the strength regime, Holsapple's cratering efficiency π_v, defined as the ratio excavated crater and impactor mass, is

$$\pi_V \propto \left(\frac{\rho V^2}{Y}\right)^{\frac{3\mu}{2}}, \tag{1}$$

where ρ is target density, V is impact velocity and Y the material strength of the target. Assuming that the surface material (density and material strength) of the sub-km sized crater on the Moon is the same as that of our experimental target, Eq. (1) can be rewritten as

$$\pi_V \propto V^{3\mu}. \tag{2}$$

For various rock targets (containing brittle ones), μ has a constant value of 0.55 (Holsapple, 1993). Hence, Eq. (2) can be rewritten as

$$\pi_V \propto V^{1.65}. \tag{3}$$

As the cube of D/L (the crater-to impactor diameter ratio) equals π_v, which can be rewritten as

$$\frac{D}{L} \propto \pi_V^{\frac{1}{3}}. \tag{4}$$

A cratering efficiency of $D/L = 8.19$ for our set of experiments can be derived from the data of shot s1941, with crater diameter at vertical impact $D = 5.85$ cm and impactor diameter $L = 0.714$ cm. As pointed out above, cratering efficiency is itself a function of impact angle, so we normalized it with regard to the cratering efficiency of the corresponding vertical impact event D, as proposed by Collins et al. (2011). In shot s1941, the impact velocity is 2.44 km/s. Therefore, combining this value, Eq. (3) and Eq. (4), the cratering efficiency D/L at an arbitrary impact velocity V [km/s] can be estimated by

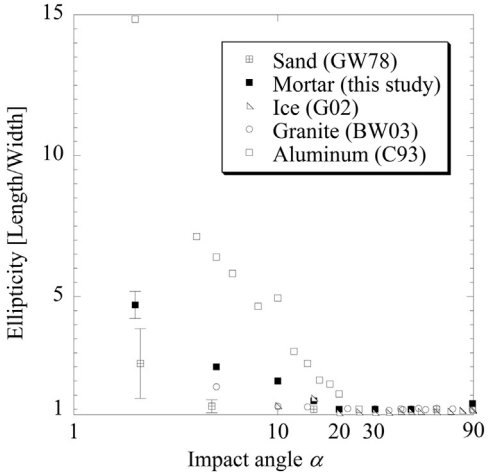

Fig. 9. Ellipticity of craters vs impact angle, plotted for the laboratory impact experiments of GW78 (Gault and Wedekind, 1978), this study, G02 (Grey et al., 2002), BW03 (Burchell and Whitehorn, 2003) and C93 (Christiansen et al., 1993). GW78 fired aluminum and pyrex spheres into sand targets at 6.4 km/s; We fired nylon projectile spheres into mortar targets at a nominal velocity of 2.3 km/s; G02 fired aluminum spheres into ice targets at nominal velocity of 5.2 km/s; BW03 fired stainless-steel spheres into granite targets at nominal velocity of 5.4 km/s, whilst C93 fired aluminum spheres into aluminum targets at 6.5–7.0 km/s. For this study, the data of the craters obtained from shots at an impact angle of 5°-90° in targets without a cavity and s1711 (with an impact angle of 2°) were used. C93 did not indicate error bars in their paper. For most of the other data, error bars are generally smaller than symbol size.

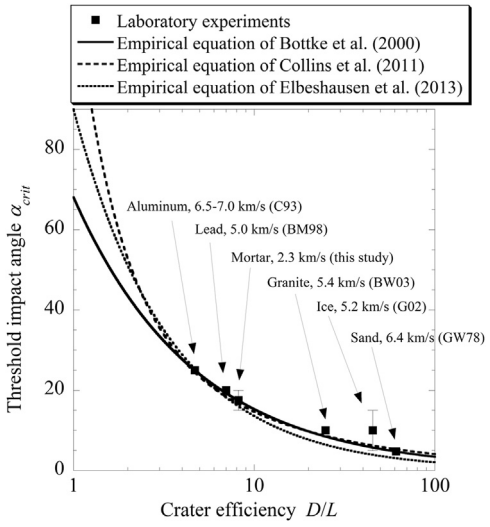

Fig. 10. Threshold angle of the transition from circular to elliptic crater as a function of cratering efficiency (the ratio of crater diameter to projectile diameter in the vertical impact case D/L). According to Collins et al. (2011), cratering efficiency is itself a function of the impact angle. Therefore, we normalized it with regard to the cratering efficiency of the corresponding vertical impact event D, as proposed in their study. Six experimental data points are plotted as solid squares. The threshold impact angles in ice and our mortar were assumed to be 10° and 17.5°, i.e. the mean of 5° and 15° and the mean of 15° and 20°, respectively. Lead experimental data of BM98 (Burchell and Mackay, 1998) was added to include another metal target. BM98 fired stainless steel spheres into lead targets at nominal velocity of 5.2 km/s. Three empirical equations are indicated as fitting functions for the data of those laboratory experiments. These are empirical equations of Bottke et al. (2000), Collins et al. (2011) and Elbeshausen et al. (2013): $\alpha_{crit} = 68.1°\left(\frac{D}{L}\right)^{-0.648}$, $\alpha_{crit} = 45°\left(\frac{D}{L}\right)^{-0.52} + 77°\left(\frac{D}{L}\right)^{-1.85}$ and $\alpha_{crit} = 90°\left(\frac{D}{L}\right)^{-0.82}$, where α_{crit} is the threshold impact angle.

$$\frac{D}{L} = 8.19\left(\frac{V}{2.44}\right)^{0.55}. \quad (5)$$

On the other hand, the empirical equation of the threshold impact angle α_{crit} as a function of the cratering efficiency is

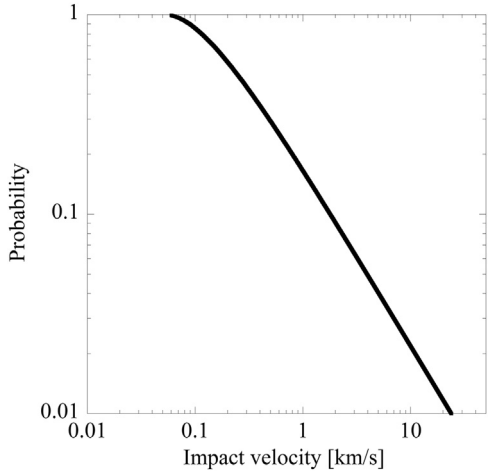

Fig. 11. Impact velocity and probability of elliptical crater formation in the strength regime, which is obtained from our experimental data, the empirical equation of Elbeshausen et al. (2013) and the scaling law of Holsapple (1993).

$$\alpha_{crit} = 90°\left(\frac{D}{L}\right)^{-0.82}, \quad (6)$$

where we used the equation of Elbeshausen et al. (2013). Other equations have been proposed but Eq. (6) is simple and not too different. Substituting Eq. (5) into Eq. (6), the relation between threshold angle α_{crit} and impact velocity can be determined.

For planetary impactors approaching from random directions, the frequency function dP for the impact angle of α is $dP = \sin 2\alpha\ d\alpha$ (Shoemaker, 1962). This means that, the probability P of a meteoroid impact into a planetary target surface at the impact angle less than α can be expressed as

$$P = \frac{1}{2}(1 - \cos 2\alpha). \quad (7)$$

Using this equation and the estimate above, the probability of the formation of elliptical craters at arbitrary impact velocities can be estimated as shown in Fig. 11.

Fig. 11 indicates that the probability of the elliptical crater formation in the strength regime increases with decreasing impact velocity. The estimated average impact velocity on the Moon ranges from 16 to 22 km/s (Ivanov, 2001; Le Feuvre and Wieczorek, 2008; Ito and Malhotra, 2010; Yue et al., 2013). In fact, the impact velocities of almost all meteoroids producing primary craters are greater than several km/s (Ivanov, 2001; Ito and Malhotra, 2010; Yue et al., 2013). At velocities in this range, the probability of the elliptical crater formation in the strength regime is very low, less than a few percent. In contrast, because the impact velocity producing secondary craters on the Moon is generally considered to be several hundred meters per second (e.g., Hirata and Nakamura, 2006), the probability of elliptical crater formation in this velocity range is several tens of percent. It is therefore conceivable that most craters in the 100 m size range, including a pit crater on the Moon, having an elliptical shape, are in fact secondary craters.

The amount of spacecraft imagery related to a hundred meter sized lunar craters has been steadily increasing. The age of surface features on the Moon is occasionally determined using statistical data of craters in the sub-km size range (e.g., Hiesinger et al., 2003; Morota et al., 2011). However, the ratio of secondary craters to primary craters in this size range is poorly understood, although the ratio of the secondary craters to primary craters is likely to increase with decreasing crater size (e.g., Nagumo and Nakamura, 2001; Robbins and Hynek, 2014). Some researchers even tend to avoid using $D < 1$ km impact craters, partly to avoid secondary crater contamination. This is why investigating the ratio of secondary craters to primary craters in the sub-km range

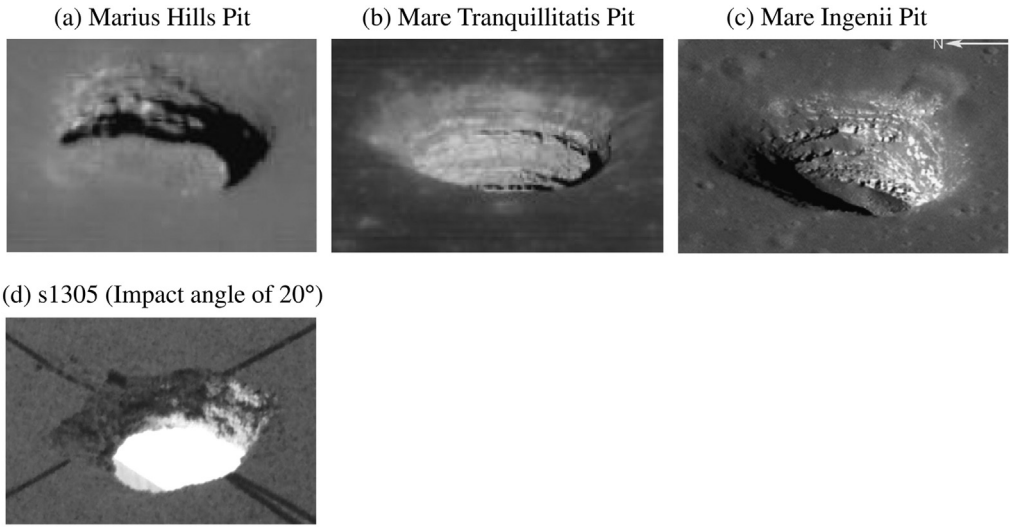

Fig. 12. Oblique views of the relatively large pit craters on the Moon and shot s1305 in this experiment. (a) Marius Hills Pit (34° incidence angle; M137929856R). (b) Mare Tranquillitatis Pit (11° incidence angle; M155023632R). (c) Mare Ingenii Pit (44° incidence angle; M184810930L). Images taken from Robinson et al. (2012). (d) Oblique view of experimental shot s1305.

is very important to accurately date lunar surface features.

4.3. Implications for pit craters on the Moon

Craters in the 100 m size range are more likely to be elliptical, although the data available at the time of this writing is not sufficient to show the tendency. For instance, the three pit craters on the Moon are elliptical and their ellipticities range from 1.2 to 1.6 (Robinson et al., 2012). Viewed from oblique angles, we can see that the topography of the front crater and the hole in shot s1305 (Fig. 12) resembles the lunar pit craters. One has to bear in mind that, in our experiments, the size and shape of craters at a given impact angle are similar, regardless of the existence of a hole. Thus, the relation shown in Fig. 11 would be applicable to the three pit craters on the Moon. Besides, in our experiments, the ellipticities of the front crater and the hole are similar at a given impact angle. Hence, the ellipticities of the pit craters on the Moon can be considered to reflect the shape of the original crater, even though the collapse of the remaining roof might have exceeded the original crater shape. Consequently, it is quite natural that the pit craters on the Moon are elliptical.

5. Conclusions

We investigated the effect of impact angle on crater ellipticity in the strength regime to understand the formation of lunar elliptical craters in the 100 m size range. For this purpose, we carried out oblique impact cratering experiments on mortar targets with and without a cavity using a two-stage light-gas gun. The ellipticities of the craters increase dramatically with decreasing impact angle once it falls below a threshold angle of 15°-20°, which is in line with Bottke et al. (2000), Collins et al. (2011) and Elbeshausen et al. (2013) that the threshold angle for the formation of elliptical craters is a function of cratering efficiency.

In targets with a cavity, a crater (rear crater) was produced on the opposite side of the target with respect to the impact. Penetration of the target was achieved when front and rear craters were connected to form a continuous hole. While the widths of front crater, rear crater and hole were found to decrease with decreasing the impact angle, the lengths of front crater and hole remain largely constant regardless of impact angle. As a result, the ellipticities of front crater and hole are similar, and increase with decreasing impact angle. The ellipticity of the rear crater on the other hand remains roughly constant regardless of the impact angle as its length decreases slightly with decreasing impact angle. We also found that, for a given impact angle, the sizes and shapes of the craters in both types of targets are similar, regardless of the existence of a hole. Applying our experimental results to three pit craters on the Moon we note that the topographies of these pit craters, although not very accurately known, appear to be similar to those craters with a hole in our experiments.

We then examined the relation between impact velocity and probability of elliptical crater formation using our experimental data and previous empirical equation. We found that the probability of elliptical crater formation at an average impact velocity of 16–20 km/s on the Moon is very low, less than a few percent. On the other hand, the probability of elliptical crater formation at impact velocities of several hundred meters per second (which is same velocity producing secondary crater) is several tens of percent. We therefore conclude that most of the elliptical craters produced in the strength regime are likely to be secondary craters.

Acknowledgements

The authors acknowledge Akifumi Yoshida and Ryota Kobayashi for the support of their experiments. The experiments described in this paper were conducted and supported by ISAS/JAXA in collaboration with the Hypervelocity Impact Facility (former facility name: the Space Plasma Laboratory). This paper was significantly improved by the comments from two anonymous reviewers. AH would like to acknowledge financial support by STFC under grant number ST/L000776/1.

References

Bottke, W.F., Love, S.G., Tytell, D., Glotch, T., 2000. Interpreting the elliptical crater populations on Mars, Venus and the Moon. Icarus 145, 108–121.
Burchell, M.J., Mackay, N.G., 1998. Crater ellipticity in hypervelocity impacts on metals. J. Geophys. Res. 103 (E10), 22761–22774.
Burchell, M.J., Whitehorn, L., 2003. Oblique incidence hypervelocity impacts on rock. Mon. Not. R. Astron. Soc. 341, 192–198.
Christiansen, E.L., Cykowski, E., Ortega, J., 1993. Highly oblique impacts into thick and thin targets. Int. J. Impact Eng. 14, 157–168.
Collins, G.S., Elbeshausen, D., Davison, T.M., Robbins, S.J., Hynek, B.M., 2011. The size-frequency distribution of elliptical impact craters. Earth Planet. Sci. Lett. 310, 1–8.
Cushing, G.E., 2012. Candidate cave entrances on Mars. J. Cave Karst Stud. 74, 33–47.
Daubar, I.J., Atwood-Stone, C., Byrne, S., McEwen, A.S., Russell, P.S., 2014. The morphology of small fresh craters on Mars and the Moon. J. Geophys. Res. 119, 2620–2639. http://dx.doi.org/10.1002/2014JE004671.
Elbeshausen, D., Wünnemann, K., Collins, G.S., 2009. Scaling of oblique impacts in frictional targets: implications for crater size and formation mechanisms. Icarus 204, 716–731.
Elbeshausen, D., Wünnemann, K., Collins, G.S., 2013. The transition from circular to

elliptical impact craters. J. Geophys. Res. 118, 2295–2309. http://dx.doi.org/10.1002/2013JE004477.
Gault, D.E., 1973. Displaced mass depth, diameter, and effects of oblique trajectories for impact craters formed in dense crystalline rocks. The Moon 6, 32–44.
Gault, D.E., Wedekind, J.A., 1978. Experimental studies of oblique impact. Proc. Lunar Planet. Sci. 9, 3843–3875.
Grey, I.D.S., Burchell, M.J., Shrine, N.R.G., 2002. Scaling of hypervelocity impact craters in ice with impact angle. J. Geophys. Res. 107 (E10), 5076. http://dx.doi.org/10.1029/2001JE001525.
Haruyama, J., Hioki, K., Shirao, M., Morota, T., Hiesinger, H., van der Bogert, C.H., Miyamoto, H., Iwasaki, A., Yokota, Y., Ohtake, M., Matsunaga, T., Hara, S., Nakanotani, S., Pieters, C.M., 2009. Possible lunar lava tube skylight observed by SELENE cameras. Geophys. Res. Lett. 36, L21206. http://dx.doi.org/10.1029/2009GL040635.
Haruyama, J., Morota, T., Kobayashi, S., Sawai, S., Lucey, P.G., Shirao, M., Nishino, M.N., 2012. Lunar holes and lava tubes as resources for lunar science and exploration. In: Badescu, V. (Ed.), Moon - Prospective Energy and Material Resources. Springer, Berlin Heidelberg, 139–163.
Hiesinger, H., Head, J.W., Wolf, U., Jaumann, R., Neukum, G., 2003. Ages and stratigraphy of mare basalts in Oceanus Procellarum, Mare Nubium, Mare Cognitum, and Mare Insularum. J. Geophys. Res., 108. http://dx.doi.org/10.1029/2002JE001985.
Hirata, N., Nakamura, A.M., 2006. Secondary craters of Tycho: Size-frequency distributions and estimated fragment size–velocity relationships. J. Geophys. Res. 111, E03005. http://dx.doi.org/10.1029/2005JE002484.
Holsapple, K.A., Schmidt, R.M., 1979. A material-strength model for apparent crater volume. Proc. Lunar Planet. Sci. 10, 2757–2777.
Holsapple, K.A., 1993. The scaling of impact processes in planetary science. Annu. Rev. Earth Planet. Sci. 21, 333–373.
Ito, T., Malhotra, R., 2010. Asymmetric impacts of near-Earth asteroids on the Moon. Astron. *Astrophys.* 519, A63.
Ivanov, B.A., 2001. Mars/Moon cratering rate ratio estimates. Space Sci. Rev. 96, 87–104.
Le Feuvre, M., Wieczorek, M.A., 2008. Nonuniform cratering of the terrestrial planets. Icarus 197, 291–306.
Martellato, E., Foing, B.H., Benkhoff, J., 2013. Numerical modeling of impact crater formation associated with isolated lunar skylight candidates on lava tubes. Planet Space Sci. 86, 33–44.
Melosh, H.J., 1989. Impact Cratering: A Geologic Process. Oxford University Press, New York.
Michikami, T., Hargermann, A., Miyamoto, H., Miura, S., Haruyama, J., Lykawka, P.S., 2014. Impact cratering experiments in brittle targets with variable thickness: Implications for deep pit craters on Mars. Planet Space Sci. 96, 71–80.
Morota, T., Haruyama, J., Ohtake, M., Matsunaga, T., Honda, C., Yokota, Y., Kimura, J., Ogawa, Y., Hirata, N., Demura, H., Iwasaki, A., Sugihara, T., Saiki, K., Nakamura, R., Kobayashi, S., Ishihara, Y., Takeda, H., Hiesinger, H., 2011. Timing and characteristics of the latest mare eruption on the Moon. Earth Planet. Sci. Lett. 302, 255–266.
Nagumo, K., Nakamura, A.M., 2001. Reconsideration of crater size-frequency distribution on the moon: effect of projectile population and secondary craters. Adv. Space Res. 28, 1181–1186.
Robbins, S.J., Hynek, B.M., 2014. The secondary crater population of Mars. Earth Planet. Sci. Lett. 400, 66–76.
Robinson, M.S., Ashley, J.W., Boyd, A.K., Wagner, R.V., Speyerer, E.J., Ray Hawke, B., Hiesinger, H., van der Bogert, C.H., 2012. Confirmation of sublunarean voids and thin layer in mare deposits. Planet Space Sci. 69, 18–27.
Schulson, E.M., 1999. The structure and mechanical behavior of ice. J. Miner. Met. Mater. Soc. 51 (2), 21–27.
Shoemaker, E.M., 1962. Interpretation of lunar craters. In: Kopal, Z. (Ed.), Physics and Astronomy of the Moon. Academic, New York, 283–359.
Stöffler, D., Ryder, G., Ivanov, B.A., Artemieva, N.A., Cintala, M.J., Grieve, R.A.F., 2006. Cratering history and lunar chronology. Rev. Mineral. Geochem. 60, 519–596.
Yue, Z., Johnson, B.C., Minton, D.A., Melosh, H.J., Di, K., Hu, W., Liu, Y., 2013. Projectile remnants in central peaks of lunar impact craters. Nat. Geosci. 6, 435–437.